Received: 29 September 2022 | Revised: 23 June 2023 | Accepted: 4 July 2023

DOI: 10.1002/mp.16648

RESEARCH ARTICLE

MEDICAL PHYSICS

Multiparametric ultrasound imaging for early-stage steatosis: Comparison with magnetic resonance imaging-based proton density fat fraction

Jihye Baek[1] | **Lokesh Basavarajappa**[2] | **Ryan Margolis**[2] | **Leroy Arthur**[2] | **Junjie Li**[2] | **Kenneth Hoyt**[2] | **Kevin J. Parker**[1]

[1]Department of Electrical and Computer Engineering, University of Rochester, Rochester, New York, USA

[2]Department of Bioengineering, University of Texas at Dallas, Richardson, Texas, USA

Correspondence
Kevin J. Parker, University of Rochester, 724 Computer Studies Building, Box 270231, Rochester, NY 14627-0231, USA.
Email: kevin.parker@rochester.edu

Funding information
NIH, Grant/Award Numbers: R21EB025290, R01DK126833; Cancer Prevention Research Institute of Texas (CPRIT), Grant/Award Number: RP180670

Abstract

Background: The prevalence of liver diseases, especially steatosis, requires a more convenient and noninvasive tool for liver diagnosis, which can be a surrogate for the gold standard biopsy. Magnetic resonance (MR) measurement offers potential, however ultrasound (US) has better accessibility than MR.

Purpose: This study aims to suggest a multiparametric US approach which demonstrates better quantification and imaging performance than MR imaging-based proton density fat fraction (MRI-PDFF) for hepatic steatosis assessment.

Methods: We investigated early-stage steatosis to evaluate our approach. An in vivo (within the living) animal study was performed. Fat inclusions were accumulated in the animal livers by feeding a methionine and choline deficient (MCD) diet for 2 weeks. The animals ($n = 19$) underwent US and MR imaging, and then their livers were excised for histological staining. From the US, MR, and histology images, fat accumulation levels were measured and compared: multiple US parameters; MRI-PDFF; histology fat percentages. Seven individual US parameters were extracted using B-mode measurement, Burr distribution estimation, attenuation estimation, H-scan analysis, and shear wave elastography. Feature selection was performed, and the selected US features were combined, providing quantification of fat accumulation. The combined parameter was used for visualizing the localized probability of fat accumulation level in the liver; This procedure is known as disease-specific imaging (DSI).

Results: The combined US parameter can sensitively assess fat accumulation levels, which is highly correlated with histology fat percentage ($R = 0.93$, p-value < 0.05) and outperforms the correlation between MRI-PDFF and histology ($R = 0.89$, p-value < 0.05). Although the seven individual US parameters showed lower correlation with histology compared to MRI-PDFF, the multiparametric analysis enabled US to outperform MR. Furthermore, this approach allowed DSI to detect and display gradual increases in fat accumulation. From the imaging output, we measured the color-highlighted area representing fatty tissues, and the fat fraction obtained from DSI and histology showed strong agreement ($R = 0.93$, p-value < 0.05).

Conclusions: We demonstrated that fat quantification utilizing a combination of multiple US parameters achieved higher performance than MRI-PDFF; therefore, our multiparametric analysis successfully combined selected features for hepatic steatosis characterization. We anticipate clinical use of our proposed multiparametric US analysis, which could be beneficial in assessing steatosis in humans.

KEYWORDS
fat quantification, H-scan, multiparametric analysis, steatosis, tissue characterization, ultrasound

1 | INTRODUCTION

The worldwide epidemic of obesity and fatty liver disease has motivated the search for reliable, noninvasive, and widely available measures of fat in the liver.[1–3] In the past, liver biopsy has been regarded as the gold standard for assessment, however the disadvantages of this procedure include sampling error, poor patient acceptance for repeat examinations, and bleeding.[4–6] Thus, as a noninvasive surrogate for biopsy, magnetic resonance (MR) imaging techniques have gained acceptance as a quantitative and reliable standard for assessment of liver fat.[7] MR imaging-based proton density fat fraction (MRI-PDFF) has emerged as an important measurement in liver studies with the best diagnostic performance among non-invasive imaging modalities.[8] However, its high cost and long operation time limit the widespread use of MR in the clinic.

Within medical ultrasound (US), which is noninvasive and more widely available due to its more than ten times lower cost than MR or computed tomography scans, a relevant trend for addressing the quantification of liver fat is the increasing number of parameters related to compression and shear wave phenomena that can be implemented on clinical scanners in addition to analysis of ultrasound backscattering. A commonly used US image characteristic of fat accumulation is hyperechoic speckles compared to normal livers. Further analysis of the speckle distribution has been conducted while modeling the distribution with statistical models, starting from the classical Rayleigh[9] to the more recently adapted Nakagami[10] and Burr distribution.[11] Moreover, quantitative ultrasound (QUS) parameters[12] were developed and applied to tissue characterization, including the frequency spectrum analysis. These have resulted in a number of techniques and metrics for fatty liver diseases which are reviewed in recent publications.[13,14] Shear wave elastography (SWE) can also noninvasively extract attenuation and speed parameters. SWE utilizes an US push beam to generate shear waves in order to measure tissue stiffness. Previous studies[15,16] found that the SWE parameters are capable of estimating fat accumulation, but the parameters can be only measured within a limited lateral field of view and within limited penetration. Lastly, H-scan is a novel US quantification method utilizing a frequency spectral-based analysis.[17,18] It has been reported that the H-scan outperformed SWE in liver tissue characterization[19]; for differentiation between early- and mid-stage tumors, the H-scan showed significant difference (p-value < 0.0001), whereas SWS was unable to differentiate these stages (p-value > 0.05). The H-scan can characterize tissue structures related to scatterer sizes and frequency shifts, and thus can differentiate fat accumulation levels.[20]

However, generally speaking, the single-parameter correlations with steatosis suffer from imprecision in measurements, biological variability, and the inevitable presence of confounding cofactors that are unmeasured yet can influence the parameter being studied. Therefore, recent research utilizes multiparametric analysis,[21–23] whereby multiple parameters are measured simultaneously, which can improve the assessment of the degree of steatosis.[20,24–28] In these studies, the a priori classification of training sets play an important role in defining clusters of parameter values associated with a condition, and the boundaries between different states.

In this paper, we add to our previous work[20] on an animal model of steatosis by adding an independent measure of liver fat content from MR imaging as a reference. Furthermore, we focus more on short-term accumulation of liver fat at 1 and 2 weeks on a diet known to produce steatosis. We also examine the results of utilizing different subsets of measured parameters, an important consideration since not all measured parameters are equally sensitive to the accumulation of fat in the liver. Finally, we introduce a mathematical measure in multiparametric space that enables small regions of the B-scan to be assessed for degree of steatosis, leading to a color overlay forming a visual map of the degree of severity of steatosis within any individual liver. These approaches combined allow for final classification accuracies of 100% in discriminating between normal livers and those exposed to the steatotic diet at 1 and 2 weeks. The multiparametric analysis results were compared with MR and histology to evaluate performance.

2 | MATERIALS AND METHODS

2.1 | Animal model and study overview

This study protocol was approval by the Institutional Animal Care and Use Committee (IACUC) at the University of Texas at Dallas. Animal studies were conducted using Sprague-Dawley rats ($n = 19$; Charles River Laboratories, Wilmington, MA). The rats were randomly divided into control ($n = 7$) and diet ($n = 12$) groups. The control group was fed a standard chew, whereas for the diet group, a methionine and choline deficient (MCD) diet was given to induce nonalcoholic fatty liver disease (NALFD). The rats were monitored for 2 weeks under a 12-h day/night cycle with free access to food and water.

Animal livers were imaged at week 0 (baseline), week 1, and week 2 with US and MR scanners, and the animals were sacrificed after the second week's scan for histological image analysis. Utilizing the acquired US, MR, and histology images, we extracted features that can characterize livers to assess fat accumulation. Our study design is summarized in Figure 1, and the details of this feature extraction are described in the next Sections.

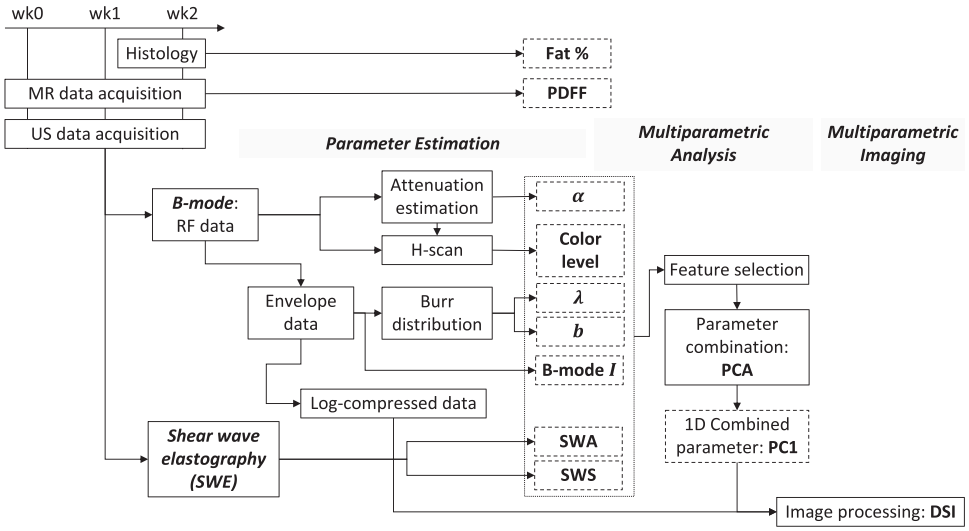

FIGURE 1 Flow diagram of study design. We acquired images or data from histology, MR, and US. Measured parameters are in dashed-line boxes. Fat %: fat percentages, PDFF: proton density fat fraction, α: attenuation coefficient, λ and b: Burr parameters, B-mode I: Brightness-mode intensity, SWA: shear wave attenuation, SWS: shear wave speed, PCA: principal component analysis, PC1: the first principal component, DSI: disease-specific imaging.

2.2 | Histology

As the ground truth for assessing steatosis progression, we quantified the fat percentages utilizing histology images. After the second week's MR and US imaging, animals were humanely euthanized, and livers were excised and sectioned for hematoxylin and eosin (H&E) staining. H&E images were binarized and processed with morphological operations using ImageJ software.[29]

2.3 | MR image acquisitions and PDFF

Liver MR imaging was performed using a 3.0 T preclinical scanner (BioSpec 3T, Bruker Corp, Billerica, MA, USA). Proton MR imaging was used to acquire signals that originate from water and fat molecules; these signals differ in frequencies because of their chemical compositions. The two-point Dixon with inhomogeneity correction method was used to acquire in-phase and out-of-phase images and to estimate an inhomogeneity phase.[30] Water-only and fat-only images were obtained at each voxel by adding and subtracting the in-phase and out-phase images after inhomogeneity correction, respectively. For this, a T2 Turbo Rare scan was used with the following imaging parameters: echo time = 50 ms and echo spacing = 10 ms. Each liver scan had a field of view (FOV) of 60 mm × 60 mm with a slice thickness of 1 mm. The fat fraction calculation was performed offline using ParaVision 360 (Bruker, Billerica, MA, USA). Rectangular regions of interest (ROI) of size 100 mm^2 were selected to avoid major blood vessels and then used to evaluate the MRI-PDFF values.

2.4 | US acquisitions and US features

We extracted 7 US features from B-mode imaging and shear wave elastography (SWE). The features were H-scan color level (H), B-mode attenuation coefficient (α), Burr distribution λ and b, B-mode intensity (B), shear wave speed (SWS), and shear wave attenuation (SWA). To measure the features from US signals, a B-mode scan was performed using a Vevo 3100 scanner (FUJIFILM VisualSonics Inc, Toronto, Canada) equipped with a 15 MHz center frequency linear probe (MX201), and then SWE was performed using the Vantage 256 US system (Verasonics Inc, Kirkland, WA, USA) equipped with an L11-4v probe. As shown in Figure 1, the B-mode imaging sequence provided radiofrequency (RF) data that were processed for H-scan analysis and attenuation estimation. In-phase quadrature (IQ) demodulation and envelope detection calculated envelope data that were processed for Burr distribution and B-mode intensity estimation. The B-mode acquired 50 or 100 frames for each scan, and every 5 frames were processed and averaged for feature measurement.

The H-scan is a matched filter analysis, extracting frequency information. Two hundred and fifty-six Gaussian filters with different peak frequencies were used for bandpass filtering in the frequency domain. These filters estimate each sample's frequency component corresponding to scatterer size. Lower to higher frequency components (larger to smaller scatterer sizes) are mapped to red and blue colors, respectively, where the red to blue range has 256 color levels from 1 to 256. However, attenuation due to US propagation causes a frequency down-shift (red-shift for the H-scan color

level) along the depth direction. Thus, we estimated the attenuation coefficient[31] prior to H-scan processing and corrected the attenuation effect in the RF data.[18] The attenuation-corrected RF data was used as the input for H-scan processing, and the estimated attenuation coefficient was used as a feature.

Utilizing envelope data which includes brightness information, we extracted three features: Burr distribution parameters λ and b, and B-mode intensity. Burr distribution fitting for a histogram of envelope data was performed to estimate λ and b. The distribution is:

$$P(A) = \frac{2A(b-1)}{\lambda^2\left[\left(\frac{A}{\lambda}\right)^2 + 1\right]^b} \quad (1)$$

where $P(A)$ is a probability density governed by the Burr distribution, and A is the envelope data amplitude. The fitting estimates are λ and b; λ is a scale factor increasing with US gain, and b is a power law exponent depending on scatterer distributions. Further, the echo amplitude is estimated by averaging the envelope data intensity which estimates B-mode intensity, which is also related to Burr λ.

A custom SWE imaging sequence consisting of three rapid push beams was implemented on the programmable Vantage 256 US system (Verasonics Inc.).[32] The push beam used an aperture size of 64 elements and a pulse length of 230 μs. The push beam was placed along the tissue depth with 2 mm spacing and in the region of liver parenchyma, avoiding major blood vessels. The induced shear waves are tracked by ultrafast plane wave imaging with a frame rate of 10 kHz. A 2-dimensional (2D) algorithm was used to calculate tissue displacement from the beamformed IQ data. Thereafter, a 2D fast Fourier transform of the tissue displacement data was used to estimate parameters of liver tissue viscoelasticity, namely the SWS and SWA.

2.5 | Multiparametric analysis and feature selection

Our goal for multiparametric analysis is to combine the individual US parameters and obtain a combined parameter which performs better than the individual US parameters, MRI-PDFF, and histology. The performance for individual parameters and the combined parameter was evaluated using a correlation coefficient (R) with its p-value, 1D support vector machine (SVM) classification accuracy, and leave-one-out cross validation (LOOCV). We extracted the seven US features and performed feature selection (Figure 2). Although we extracted the seven features, some features might not contribute to assessment of fat accumulation and classification of different fat accumulation levels, and there might be high dependence between some features. Therefore, we investigated eight feature combinations that have seven to three selected features, as listed in Figure 2. Specifically, one feature combination includes all seven features, while others exclude one–four features based on each feature's correlation coefficient with MRI-PDFF and histology fat %. The eight different combinations were selected based on each feature's R and US physics. Features with lower R were excluded but features with higher R were included. Furthermore, we tried to select conceptually independent features from distinct categories based on US physics. We extracted features based on the categories of attenuation, frequency shift information, B-mode brightness, and SWE, and thus we also investigated feature combinations including at least one feature from a category. If there were more than one feature from a category and there was high correlation between the features, one feature was included and then the others were excluded.

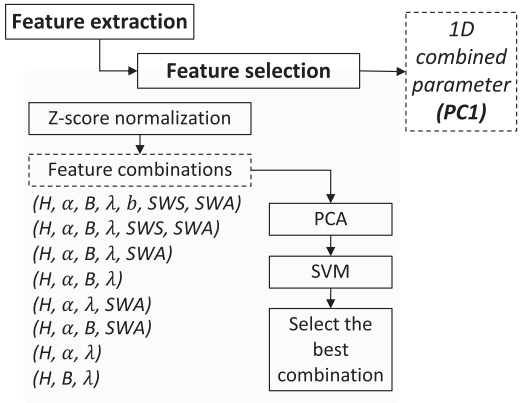

FIGURE 2 Feature selection for multiparametric analysis. H: H-scan color level, α: attenuation coefficient, B: B-mode intensity, λ and b: Burr parameters, SWS: shear wave speed, SWA: shear wave attenuation. PCA: principal component analysis, PC1: the first principal component, SVM: support vector machine.

For each feature combination, Z-score normalization was initially applied to normalize different features' scales. Using the normalized features, a principal component analysis (PCA) was performed. The first principal component (PC1) was used to calculate correlation coefficients with MRI-PDFF and histology fat percent. Using the PC1, 1D SVM classification was performed to differentiate fat accumulation levels, which can evaluate separation between classes; higher classification accuracy indicates less overlap between classes. A one-versus-the rest approach[33] was utilized for SVM classification of the three classes. Among the feature combinations, a feature set was selected, which showed higher R and less overlap between classes, and better LOOCV results (with higher accuracy and lower mean-squared error (MSE)). In this way, individual US features were combined into PC1, a combined 1D parameter, that includes information extracted from multiple parameters.

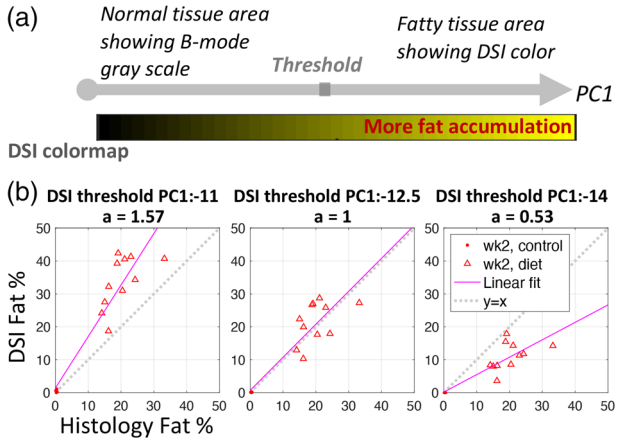

FIGURE 3 Multiparametric imaging. (A) Imaging concept with DSI colormap. PC1 is a combined parameter obtained from multiparametric analysis. A threshold differentiates normal and fatty tissue area showing B-mode gray scale and DSI color, respectively. (B) Optimization of DSI to set a threshold, which aims to provide DSI fat % consistent with ground truth histology fat %.

The performance of the selected feature set was evaluated by investigating SVM classification accuracy; the LOOCV approach was used, resulting in an averaged accuracy and MSE[34] for the different combinations of parameters.

2.6 | Multiparametric imaging—DSI

To visualize the results of the multiparametric analysis, we propose a multiparametric imaging method to provide a simple color display of the results. Beginning with the concept of disease specific imaging (DSI)[24,27] which utilizes the inner-product and the SVM, we simplify the imaging method. The combined parameter, PC1, is used for color imaging intensity, and we set a threshold to differentiate between normal and fatty tissue (Figure 3a). Fat accumulation (DSI fat area percent, *DSI fat %*) is quantified by:

$$DSI\ fat\ \% = \frac{Fatty\ tissue\ area}{Total\ area\ within\ ROI} \times 100\%. \quad (2)$$

The DSI processing is optimized by setting a threshold (*threshold PC1*) as shown in Figure 3a. The 1D SVM for PC1 can be an automatic threshold setting. However, a decision point determined by the 1D SVM relies on the training data set. Specifically, when using later-stage fatty livers for the classification between normal and fatty tissue, the threshold is further from the average PC1 of the normal class when compared to using earlier-stage fatty livers. Therefore, we set a threshold based on histology fat % instead of utilizing SVM results by solving an optimization problem. The optimization was performed by comparing the DSI fat % (y) to the ground truth histology fat % (x), and the objective function was defined by:

$$\underset{threshold\ PC1}{\text{minimize}} \ |1 - a| \quad (3)$$

subject to the constraint function of $y = ax + b$ which is a linear fit line of the scatter plot of x and y from histology fat % and DSI fat %, respectively, as shown in Figure 3b; where a is the slope and b is the intersection of the line. DSI fat % (y) can be determined by the *threshold PC1*; the fatty tissue area in Equation (2) is a set of pixels which has measures of PC1 > *threshold PC1*. Since our goal is obtaining DSI fat % comparable to the histology measurement, the objective function was defined to have a slope close to 1. Depending on the threshold, DSI can overestimate, or underestimate, fat %. Examples of overestimation and underestimation are provided in Figure 3b, in the first (*threshold PC1* $= -11$) and third (*threshold PC1* $= -14$) plots, respectively. With an optimal threshold as shown in the middle plot of Figure 3b (*threshold PC1* $= -12.5$), the linear fit line of measured data points, including control and diet groups, is almost close to the line $y = x$, indicating a slope $a = 1$.

3 | RESULTS

3.1 | Multiparametric analysis—quantification of fat accumulation

Seven individual US parameters (H, α, B, λ, b, SWS, SWA), MRI-PDFF, and histology fat % were measured, and US parameter correlation with MRI-PDFF (Figure 4) and histology fat % (Figure 5) were determined (correlation coefficient (R)). Figure 4 includes data points measured at weeks 0, 1, and 2, however Figure 5 solely provides data measured at week 2 to include histology results. As shown in Figure 4, H-scan color level showed the highest correlation with MRI-PDFF, and measurements with higher correlation in order were H, α, λ, B, SWA, SWS, and b. Burr b and SWS showed $|R|$ less than 0.1 (p-value > 0.05), which may not be able to characterize fat accumulation, and thus needs to be excluded for multiparametric analysis.

Figure 5 shows MR and US parameter correlation with histology. MRI-PDFF showed the highest $R = 0.89$ (p-value < 0.05), which is higher than the correlation coefficients for all US parameters. Thus, the MR parameter can assess fat accumulation better than the US parameters when investigating individual parameters. Among the US parameters, H-scan color level, B-mode attenuation, B-mode intensity, and Burr λ resulted in high $R > 0.8$ (p-value < 0.05). SWA was also correlated with histology fat % ($R = 0.48$, p-value < 0.05), but Burr b and SWS were not correlated with histology fat % ($|R| < 0.3$, p-value > 0.05).

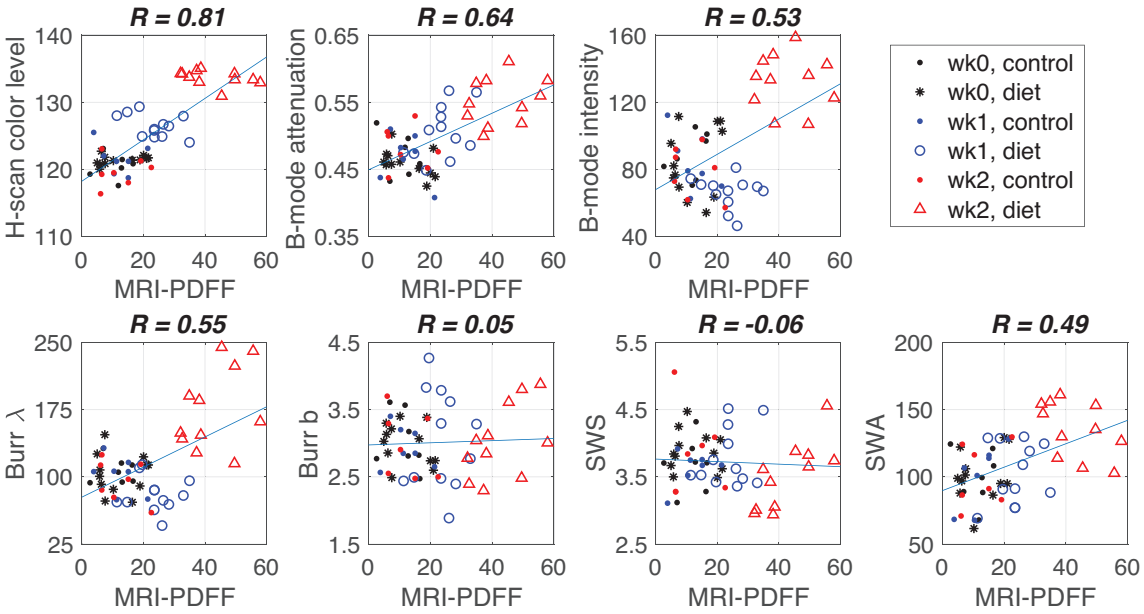

FIGURE 4 Individual US parameters and correlation (*R*, solid line) between US parameters and MRI-PDFF.

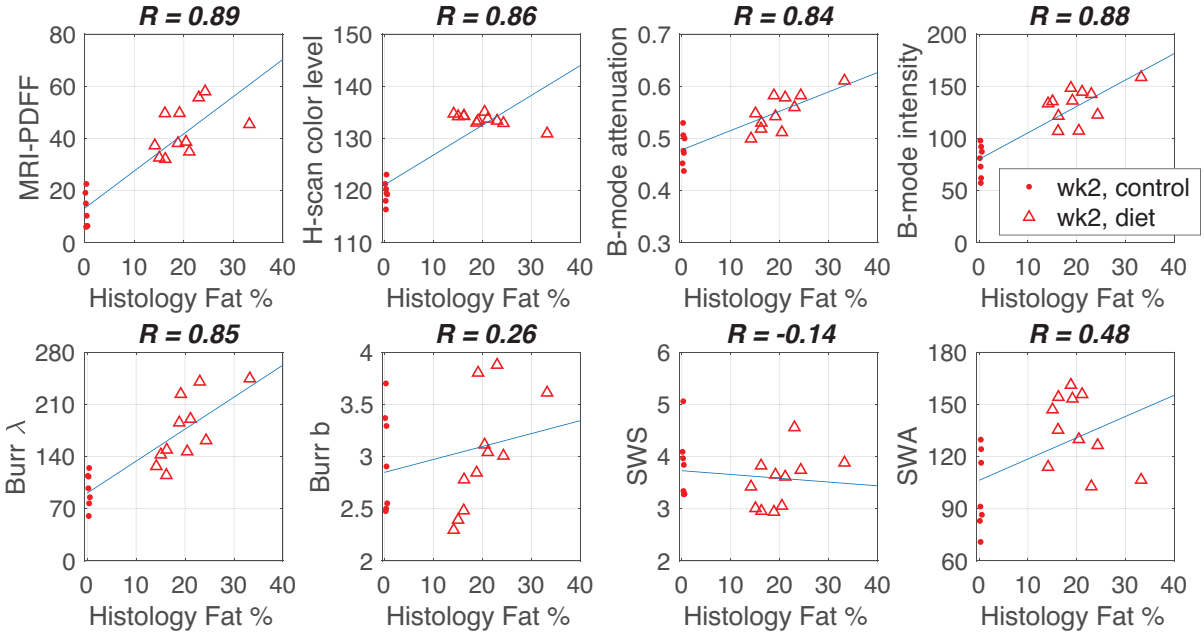

FIGURE 5 Individual US parameters and MRI-PDFF and correlation between histology and MR/US parameters. Only week 2 data are available due to histology.

3.2 | Multiparametric analysis—feature selection and a combined parameter

Eight parameter combinations were investigated as listed in Table 1. For each combination, PC1 was calculated and used to evaluate performance (correlation and SVM classification accuracy). As mentioned in Section 3.1, the correlation coefficient between MRI-PDFF and histology is 0.89 (p-value < 0.05), but correlations between PC1 and histology resulted in equal to or over 0.9 (p-value < 0.05). The highest R is 0.94 (p-value < 0.05). Therefore, our multiparametric analysis suggesting the combined parameter PC1 achieved better performance in assessing fat accumulation compared with the MR parameter. Further evaluation results of performance are provided in Table 1. To select the

TABLE 1 Feature combinations and performance for feature selection from this limited set of livers.

Parameter combination	# feature[a]	|R| Histology[b] (Week 2)	|R| MR[c] (Weeks 0,1,2)	1D SVM %[d] (GT[e]: Histology -Week 2)	1D SVM %[d] (GT[e]: MR-PDFF -Weeks 0,1,2)	3D SVM % LOOCV[f]		
						Training accuracy %	Testing accuracy %	MSE
(H, α, B, λ, b, SWS, SWA)	7	0.93	0.82	100	91.07	100	100	0
(H, α, B, λ,SWS, SWA)	6	0.93	0.82	100	91.07	100	100	0
(H, α, B, λ, SWA)	5	0.93	0.83	100	92.86	100	100	0
(H, α, B, λ)	4	0.94	0.83	100	94.64	100	100	0
(H, α, λ, SWA)	4	0.93	0.84	100	100	100	100	0
(H, α, B, SWA)	4	0.90	0.83	100	98.21	100	100	0
(H, α, λ)	3	0.94	0.84	100	98.21	100	100	0
(H, B, λ)	3	0.92	0.81	100	83.93	99.87	96.43	0.3574
…								
(λ, b, SWA)	3	0.83	0.56	83.33	69.64	78.38	71.43	0.4486
(b, SWS, SWA)	3	0.15	0.23	61.11	62.50	68.34	67.85	0.6486

Shading indicates the selected combination for multiparametric study. All correlation coefficients in this table have p-value < 0.05. Higher accuracy of 1D SVM indicates less overlap between clusters of the fat classes. LOOCV evaluated the performance of fat quantification in higher dimensional space and is illustrated in Figure 7.
[a]# feature: number of features.
[b]|R| Histology: correlation |R| with histology.
[c]|R| MR: correlation |R| with MRI-PDFF.
[d]SVM %: SVM accuracy %.
[e]GT: ground truth.
[f]LOOCV: leave-one-out cross validation.

best combination, we investigated the correlation with the ground truth histology (|R| Histology). Further, the correlation with MRI-PDFF (|R| MR) was investigated because MRI-PDFF can be used as a biomarker to quantify fat fraction with high performance.[8] In addition to the correlations, we also evaluated performance of the combined parameter by examining how much the 1D measurements overlap between different classes. The overlapped intervals were evaluated using 1D SVM, and thus all data were used as inputs of 1D SVM. The 1D SVM classification outputs can quantify the overlap; less overlapped data between classes resulted in higher classification accuracies. Furthermore, LOOCV results with SVM classification accuracy and MSE were provided for all investigated combinations. Since we first selected the eight combinations in Figure 2 based on each feature's R and US physics, their performances seemed high for all combinations; the bottom two rows in Table 1 provide two additional combinations, which were excluded for the eight-combination selection because they were expected to have low performance based on R and US physics.

Among the eight combinations, three representative combination results are shown in Figure 6, which provides correlation plots and 1D SVM classifications to show feature selection metrics. The right-most column in Figure 6 illustrates SVM classification and PC1 distribution in 1D space. We investigated two classifications where the upper and lower plots differentiated two classes of the normal/week two diet group and three classes of the normal/diet (week 1)/diet (week 2), respectively. The feature combination of (H, α, λ, SWA) resulted in 100% accuracy for the three-class classification without overlap between groups (Figure 6c). According to Figure 6 and Table 1, the parameter combination (H, α, λ, SWA), tended to show the best performance, and thus it was used for multiparametric analysis and imaging in this study.

Moreover, PCA calculated the second and third principal components (PC2 and PC3) in addition to PC1. The selected four features of (H, α, λ, SWA) were reduced into three parameters of PC1, PC2, and PC3, which can illustrate fat accumulation trajectories in 3D space as shown in Figure 7a. The gray and yellow dashed lines show trajectories over time for the diet group and the normal group, respectively. The yellow dashed lines showed fat accumulation trajectories from right to left. Figure 7b shows SVM classification for the three classes of week 2 diet, week 1 diet, and normal group. The 3D SVM LOOCV iterated observations of training/validation, and each iteration has 55 training data and one validation data. Representative five training/validation sets are provided in Figure 7c, and as shown in the results, all validation sets were classified correctly with the trained decision planes, meaning all iterations had 100% accuracy with MSE = 0 for (H, α, λ, SWA). Further, LOOCV results for the other combinations were provided in Table 1. Therefore, our multiparametric analysis combining the US parameters performed successfully, and we were able to assess

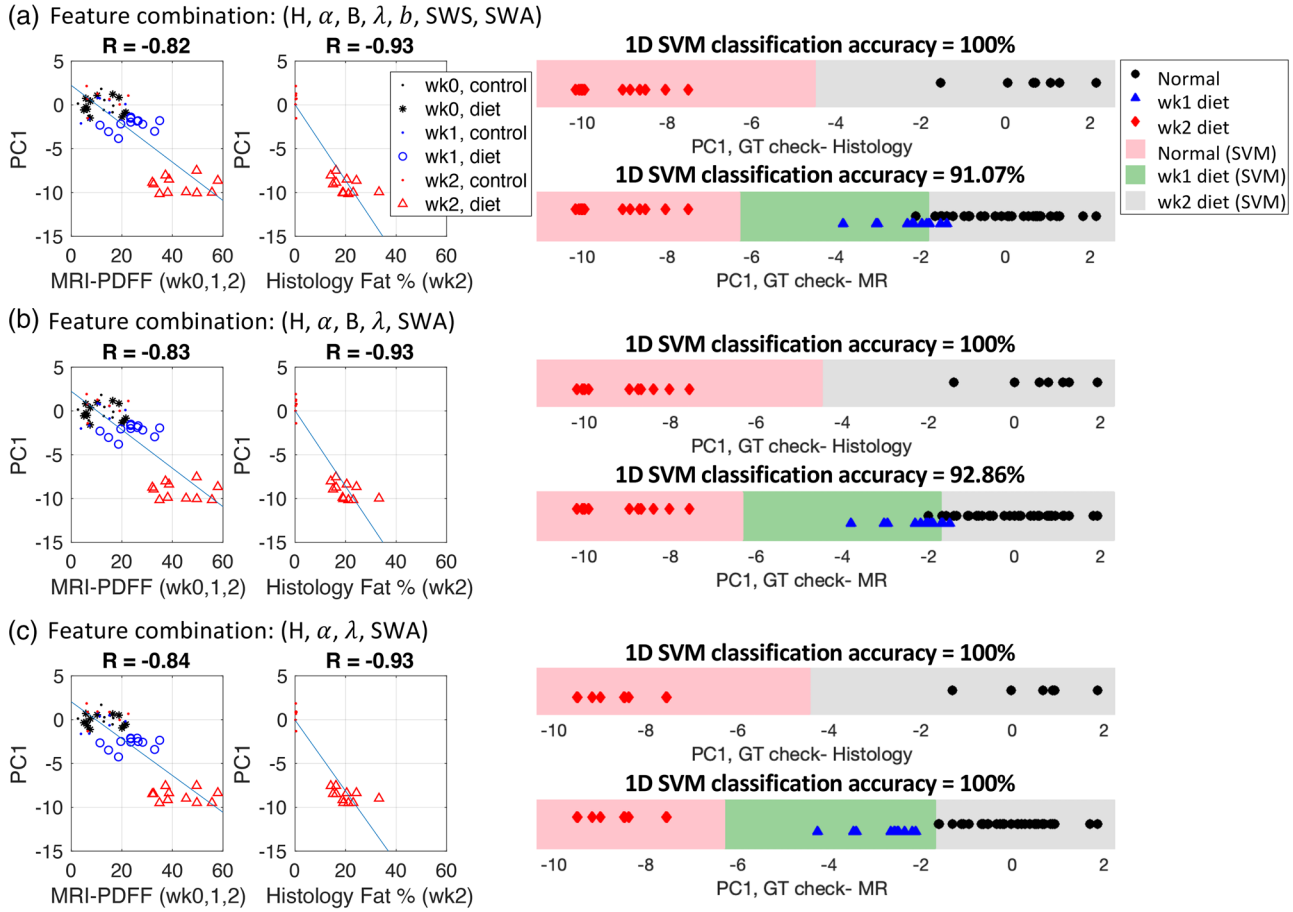

FIGURE 6 Correlation coefficients and 1D SVM accuracies for representative feature combinations, including an optimal combination. (A) includes all extracted features: (H, α, B, λ, b, SWS, SWA). (B) includes 5 features after excluding the two lowest-performing features, b and SWS: (H, α, B, λ, SWA). (C) shows the selected optimal combination of (H, α, λ, SWA). Normal (SVM), wk1 diet (SVM), and wk2 (SVM) to indicate the output of 1D SVM classification; the area boundaries denote class boundaries for the liver conditions.

progressive fat accumulation in early stages over time from week 0 to week 2.

3.3 | Multiparametric imaging—DSI

PC1 obtained from the feature combination (H, α, λ, SWA) was used for multiparametric imaging. To set a threshold to differentiate normal from fatty tissue as described in the Section 2.6. Multiparametric Imaging—DSI and Figure 3, we investigated PC1 thresholds between −15 and −10, and calculated DSI fat %. Figure 8a shows DSI optimization output with a resulting slope of a linear fitted line. Thresholds less than −12.5 underestimated fat accumulation levels as the slopes are less than 1, but thresholds greater than −12.5 overestimated fat percentages. In other words, DSI fat % is less than histology fat % for thresholds less than −12.5, whereas DSI fat % is greater than histology fat % for thresholds greater than −12.5. The PC1 threshold of −12.5 optimally estimates fat %. Figure 8b shows the measured data and its linear fit line indicating slope = 1 when using the optimal PC1 threshold of −12.5. The correlation between DSI fat % and histology fat % was $R = 0.93$ (p-value < 0.05).

Example images of B-mode, H-scan, DSI before thresholding, DSI, and MRI-PDFF are displayed in Figure 9. A DSI method is used in this study to assess and visualize fat accumulation level in livers by combining multiparametric measurements including information extracted from B-mode brightness, scatterer size, attenuation, and SWE corresponding to Burr λ, H-scan color level, attenuation coefficient α, and SWA. H-scan color level and α are local parameters; H-scan measures a color level for each pixel, whereas attenuation estimation measures α for each scanline. Burr λ and SWA are global parameters, having a measurement within a ROI. Therefore, by combining the four parameters, PC1 produces a color image DSI with pixel resolution. Figure 9 presents five liver cases with progressive fat accumulation levels from left to right; fat accumulation levels were verified by histology fat %.

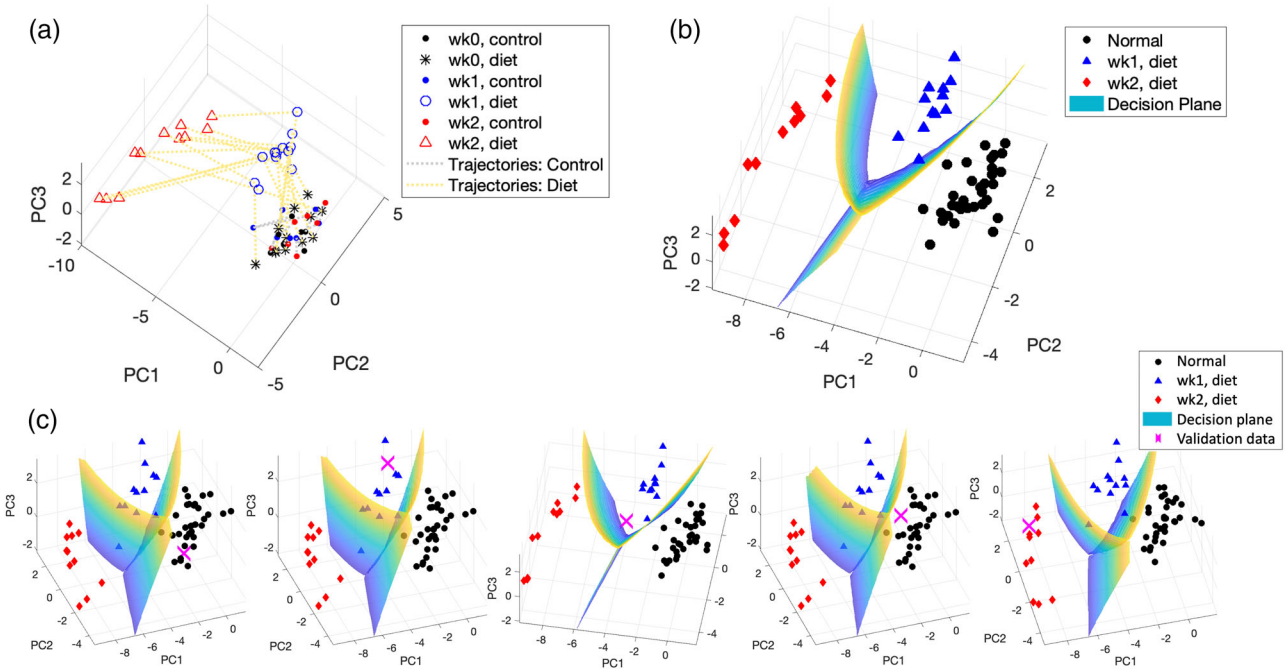

FIGURE 7 Multiparametric analysis showing (A) fat accumulation trajectories and (B) SVM classification. We appliedleave-one-out cross validation (LOOCV) to 56 data, which were divided into 55 training and 1 validation data. (C) displays 5 representative iterations of LOOCV.

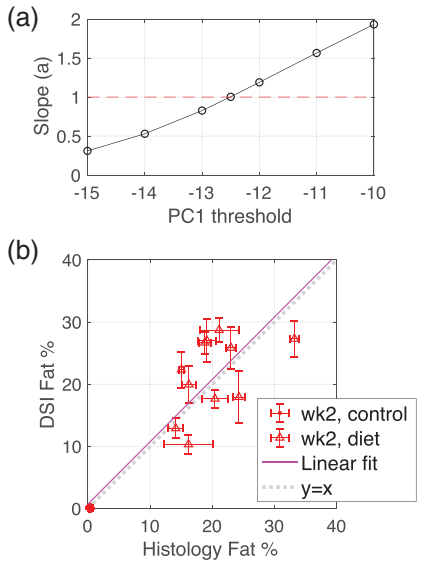

FIGURE 8 (A) DSI optimization to set an optimal threshold. (B) Correlation between DSI fat % and histology fat %.

The left-most case is a control rat at week 2, whereas the others are diet rats at week 2 with difference in histology fat %. Due to fat accumulation, B-mode and H-scan images show increase in brightness and blue color fraction, respectively. MRI-PDFF also shows increase in brightness. The image changes may not be clearly seen due to subtle differences between the B-mode, H-scan, MRI-PDFF images. However, our multiparametric analysis revealed higher performance in quantifying fat accumulation than any individual parameters, including B-mode and H-scan parameters, and thus multiparametric imaging also demonstrated more sensitive imaging illustrating fat quantification, as shown in Figure 9c,d. Figure 9c presents DSI before thresholding normal tissue area, depicting an increase in yellow color brightness from left to right; brighter yellow color can indicate a higher probability of fat accumulation. Figure 9d presents DSI results, highlighting the fatty tissue area in yellow. In addition to yellow brightness changes, the area of yellow overlay can indicate relative fat accumulation levels, so an increase in yellow overlaid area is shown from left to right. Moreover, MRI-PDFF image differences between week 2 diet rats are not clearly visible in Figure 9e. In contrast, the segmented DSI images in Figure 9d provide a better differentiation between the diet animals.

4 | DISCUSSION

Our multiparametric analysis is capable of quantifying fat accumulation levels, including early-stage steatosis induced by MCD diet for 2 weeks. This approach combined US features into a combined parameter (PC1) resulting in a correlation coefficient of $R = 0.93$ (p-value < 0.05) with histology fat quantification, outperforming the MR parameter PDFF ($R = 0.89$, p-value < 0.05). Although individual US features showed less correlation with histology compared to MRI-PDFF as shown in Figure 5, multiparametric analysis successfully combined individual parameters and achieved higher performance than MR. Utilizing the combined

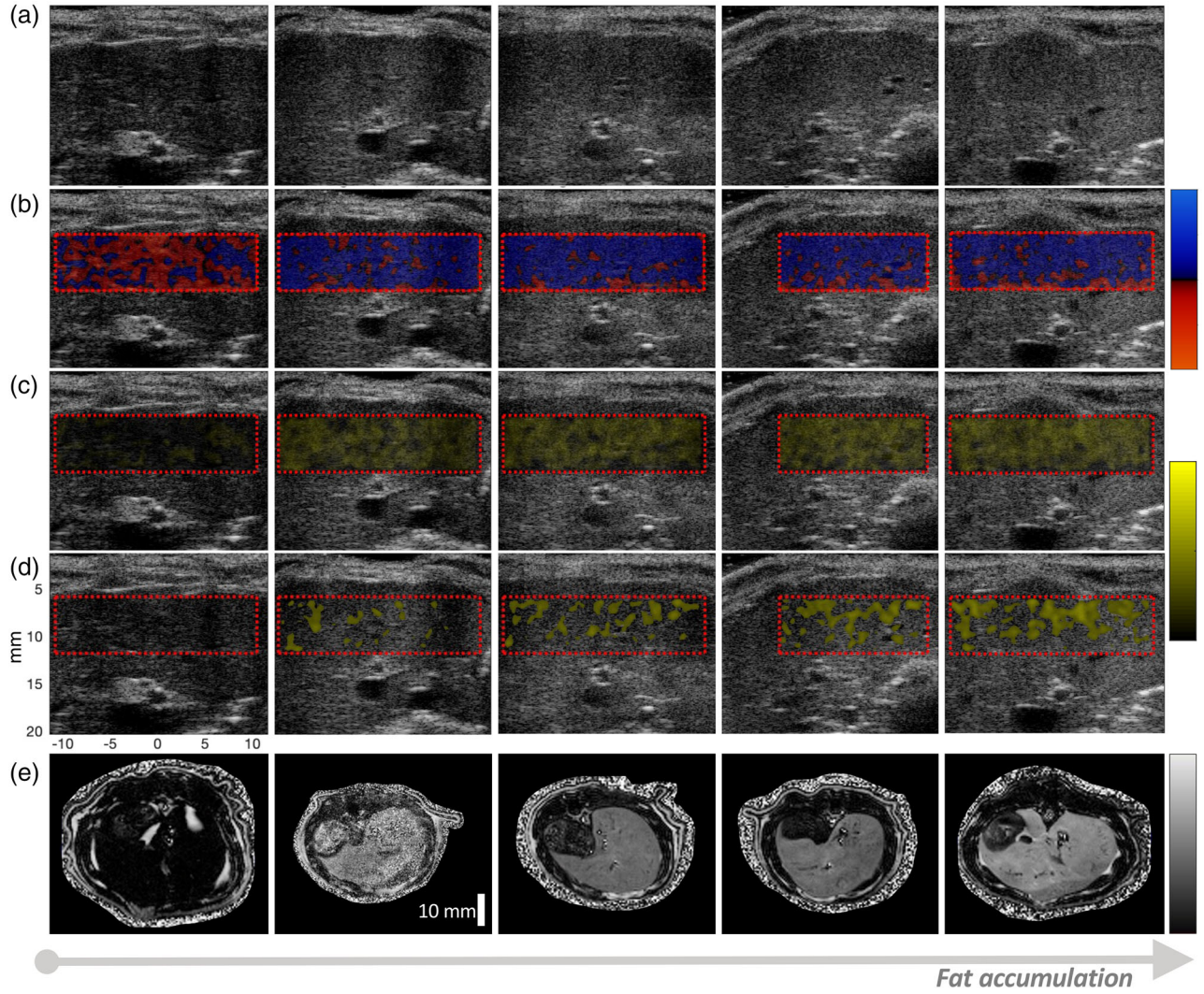

FIGURE 9 Example images of (A) B-mode, (B) H-scan, (C) DSI before thresholding, (D) DSI, and (E) MRI-PDFF for five different livers. The left column displays a control (normal) liver, and the next four columns to the right are four livers from the steatotic diet group after 2 weeks. There is increasing fat accumulation from left to right, as verified by histology, with a maximum value on the right of 33.2 percent fat. H-scan and DSI color bars are presented. The H-scan colors from red to blue indicate smaller to larger scatterer sizes. The DSI colors from dark to light yellow visualize fat accumulation levels: lighter yellow indicates more fat inclusions accumulated.

parameter, we reached 100% classification accuracy for three different fat accumulation levels (normal group and fatty liver groups at 1 and 2 weeks) as illustrated in Figure 7. Furthermore, based on the combined parameter, we suggested a multiparametric imaging framework, a simplified DSI, visualizing progressive fat accumulation by highlighting fatty tissue area as shown in Figure 9, which achieved a correlation $R = 0.93$ (p-value < 0.05) for fatty area segmentation compared to histology.

To achieve the high performance of multiparametric analysis, there are essential contributions from individual US features. This study extracted features from H-scan, attenuation estimation, B-mode backscattering, and SWE. These four categories can be considered conceptually independent. In multiparametric analysis, it is helpful to select more *independent* features. First, the H-scan analyzes the backscattered echo signals for frequency shifts and estimates scatterer sizes. The H-scan showed increase in color levels due to fat accumulation over time (Figure 4), meaning fat inclusions cause tissue structure changes resulting in a decrease in US scatterer size. Further research remains to understand how and why the fat inclusions render the US scatterer size smaller. Second, attenuation due to US beam propagation was estimated by analyzing frequency down-shift over depth. This study found that fat accumulation leads to an increase in attenuation (Figure 4). Previous studies[35–38] also reported higher attenuation in steatosis compared to normal livers. Third, backscattered US echo displayed in B-mode intensity was analyzed by measuring the intensity of B-mode envelope data and fitting the envelope data

using a Burr distribution. The envelope intensity and Burr parameter λ estimate brightness, and Burr parameter b estimates envelope histogram distribution. In this study, Burr b tended to remain unchanged as fat accumulated for the investigated early-stage steatosis, whereas the backscattering estimated by envelope intensity and Burr λ seemed to increase due to fat accumulation (Figure 4). We investigated the correlation coefficient between the measurements of envelope intensity (B) and Burr λ and found a high correlation of $R = 0.88$ (p-value < 0.05) between B and λ. Further, as reported in Table 1, we investigated parameter combinations, which include both (H, α, B, λ, SWA) and each (H, α, λ, SWA)/ (H, α, B, SWA) parameter. Including only one parameter λ instead of including two dependent parameters showed the highest performance among the three combinations. Thus, selecting independent parameters can result in a higher performing multiparametric analysis. Lastly, we extracted SWS and SWA from viscoelasticity utilizing SWE. An increase in SWA was detected due to fat accumulation, whereas SWS seemed unchanged as fat accumulated for 2 weeks (Figure 4). Thus, SWA was included but SWS was excluded for the multiparametric analysis in this study. In summary, we extracted seven relatively independent features within the four categories, and only one feature from each category was included for multiparametric study; because the combination (H, α, λ, SWA) includes all four categories considered in this study and also tended to show higher performance than the other combinations as reported in Table 1. Thus, the four categories of tissue structure changes, attenuation, backscattering, and viscoelasticity contribute to assess and quantify fat accumulation in liver. Furthermore, in multiparametric analysis, we suggest including more independent features but excluding dependent features. This results in higher performance than solely including more features without considering feature dependence. We focused on including 4 independent feature categories which have different US physics characteristics, and the evaluation metrics of the correlation coefficients and SVM classification accuracies supported our approach, showing the combination (H, α, λ, SWA) tended to outperform the others. However, note that performances between different combinations are not necessarily statistically significant. If there are combinations including only one feature among several dependent parameters (e.g., B-scan intensity and Burr λ), these combinations can perform similarly without showing significant differences. More extensive statistical analysis including post-hoc corrections on a larger set of samples would make our approach more reliable in future work.

When investigating changes in individual US parameters over time in Figure 4, H-scan color level, B-mode attenuation, and SWA tended to increase over time, indicating progressive fat accumulation; Burr b and SWS did not seem to detect fat accumulation with $|R| < 0.1$. However, the two parameters of B-mode intensity and Burr λ detecting US echogenicity decreased from week 0 to 1 and then increased from week 1 to 2. The week 1 measurements were slightly lower than the baseline. In this study, we only obtained histology images from normal livers and the week 2 diet group. Therefore, we cannot explain the week 1 results (decrease in some parameters), and further research is required.

Previous US multiparametric analyses have shown promise in the improvement of liver disease assessment.[21,22,39,40] Specifically, Pirmoazen et al.[21] showed agreement with our findings; their spectral driven parameters, attenuation coefficient, and Nakagami parameter correspond to our H-scan, attenuation coefficient, and Burr parameters, respectively. Pirmoazen et al. also reported that the SWE parameter had lower performance compared to the other parameters, which was demonstrated in our results as well. Previous multiparametric studies demonstrated quantitative assessment of performance, for example providing correlation coefficients or classification accuracies. However, we have further provided DSI, a visual display, which combines information from multiple parameters. DSI can help clinicians understand results of a multiparametric analysis without background knowledge of the parameters.

For diagnosis of hepatic steatosis, biopsy is still the gold standard. However, recently MR has been utilized to quantify fat fraction in livers due to its noninvasive nature. MRI-PDFF is one of the most used MR quantification methods for accurate fat quantification,[41] but to become a surrogate biomarker for biopsy, further improvement is required.[42] Our noninvasive technique demonstrated higher precision in the quantification of fat accumulation than MRI-PDFF, with the advantages of lower cost and higher accessibility. Hence, with further validation of our approach, our multiparametric US analysis could have more potential than a single MR parameter (e.g., MRI-PDFF) to be an alternative to biopsy as the gold standard in assessing steatosis.

Moreover, although our multiparametric approach has been validated using US features in this paper, this approach can be applied to MR or computed tomography (CT) data. The radiomics study has been performed with multiple features, and there has been effort to combine multiple features using artificial intelligence (AI).[43] Multiparametric MR analysis for the detection of non-alcoholic fatty liver diseases was also performed.[44] Thus, some multiple features from previous studies can be utilized for the first step of "parameter estimation" in Figure 1. Then with the MR or CT features, the other two steps of "multiparametric analysis" and "multiparametric imaging" enable the application of our method to MR or CT data.

5 | CONCLUSION

Our quantification and imaging successfully assessed fat accumulation levels in early-stage hepatic steatosis, where low grade steatosis was induced for 2 weeks with fat percentages between 14% and 33%. The quantification was performed by obtaining a combined parameter from individual US features, and it resulted in a high correlation ($R = 0.93$, p-value < 0.05) with histology fat percentages, outperforming the correlation between MRI-PDFF and histology ($R = 0.89$, p-value < 0.05). Moreover, the suggested DSI can illustrate the probability of fat accumulation locally in the liver. This simple visual display could provide clinicians with a more convenient steatosis diagnosis tool since it does not require the understanding of individual US features.

ACKNOWLEDGMENTS

This work was supported by NIH grants R21EB025290 and R01DK126833, and Cancer Prevention Research Institute of Texas (CPRIT) award RP180670.

CONFLICTS OF INTEREST STATEMENT

The authors have no conflicts to disclose.

DATA AVAILABILITY STATEMENT

Data available from authors upon request.

REFERENCES

1. Browning JD, Szczepaniak LS, Dobbins R, et al. Prevalence of hepatic steatosis in an urban population in the United States: impact of ethnicity. *Hepatology*. 2004;40(6):1387-1395.
2. Diehl AM, Day C. Cause, pathogenesis, and treatment of nonalcoholic steatohepatitis. *N Engl J Med*. 2017;377:2063-2072.
3. Adams LA, Lindor KD. Nonalcoholic fatty liver disease. *Ann Epidemiol*. 2007;17(11):863-869.
4. Zhou K, Lu LG. Assessment of fibrosis in chronic liver diseases. *J Digest Dis*. 2009;10(1):7-14.
5. Colloredo G, Guido M, Sonzogni A, Leandro G. Impact of liver biopsy size on histological evaluation of chronic viral hepatitis: the smaller the sample, the milder the disease. *J Hepatol*. 2003;39(2):239-244.
6. Kleiner DE, Brunt EM, Van Natta M, et al. Design and validation of a histological scoring system for nonalcoholic fatty liver disease. *Hepatology*. 2005;41(6):1313-1321.
7. Caussy C, Reeder SB, Sirlin CB, Loomba R. Noninvasive, quantitative assessment of liver fat by MRI-PDFF as an endpoint in NASH trials. *Hepatology*. 2018;68(2):763-772.
8. Tamaki N, Ajmera V, Loomba R. Non-invasive methods for imaging hepatic steatosis and their clinical importance in NAFLD. *Nat Rev Endocrinol*. 2022;18(1):55-66.
9. Burckhardt CB. Speckle in ultrasound B-mode scans. *IEEE Trans Son Ultrason*. 1978;25(1):1-6.
10. Shankar PM. A general statistical model for ultrasonic backscattering from tissues. *IEEE Trans Ultrason Ferroelectr Freq Control*. 2000;47(3):727-736.
11. Parker KJ, Poul SS. Burr, Lomax, Pareto, and logistic distributions from ultrasound speckle. *Ultrason Imaging*. 2020;42(4-5):203-212.
12. Oelze ML, Mamou J. Review of quantitative ultrasound: envelope statistics and backscatter coefficient imaging and contributions to diagnostic ultrasound. *IEEE Trans Ultrason Ferroelectr Freq Control*. 2016;63(2):336-351.
13. Pirmoazen AM, Khurana A, El Kaffas A, Kamaya A. Quantitative ultrasound approaches for diagnosis and monitoring hepatic steatosis in nonalcoholic fatty liver disease. *Theranostics*. 2020;10(9):4277-4289.
14. Ferraioli G, Berzigotti A, Barr RG, et al. Quantification of liver fat content with ultrasound: a WFUMB position paper. *Ultrasound Med Biol*. 2021;47(10):2803-2820.
15. Sharma AK, Reis J, Oppenheimer DC, et al. Attenuation of shear waves in normal and steatotic livers. *Ultrasound Med Biol*. 2019;45(4):895-901.
16. Parker KJ, Partin A, Rubens DJ. What do we know about shear wave dispersion in normal and steatotic livers? *Ultrasound Med Biol*. 2015;41(5):1481-1487.
17. Parker K. The H-scan format for classification of ultrasound scattering. *OMICS J Radiol*. 2016;5(5):1000236.
18. Parker KJ, Baek J. Fine-tuning the H-scan for discriminating changes in tissue scatterers. *Biomed Phys Eng Expr*. 2020;6(4).
19. Baek J, Ahmed R, Ye J, Gerber SA, Parker KJ, Doyley MM. H-Scan, shear wave and bioluminescent assessment of the progression of pancreatic cancer metastases in the liver. *Ultrasound Med Biol*. 2020;46(12):3369-3378.
20. Baek J, Poul SS, Basavarajappa L, et al. Clusters of ultrasound scattering parameters for the classification of steatotic and normal livers. *Ultrasound Med Biol*. 2021;47(10):3014-3027.
21. Pirmoazen AM, Khurana A, Loening AM, et al. Diagnostic performance of 9 quantitative ultrasound parameters for detection and classification of hepatic steatosis in nonalcoholic fatty liver disease. *Invest Radiol*. 2022;57(1):23-32.
22. Han A, Boehringer AS, Zhang YN, et al. Improved assessment of hepatic steatosis in humans using multi-parametric quantitative ultrasound. Paper presented at: 2019 IEEE International Ultrasonics Symposium (IUS). 2019.
23. Sanabria SJ, Pirmoazen AM, Dahl J, Kamaya A, El Kaffas A. Comparative study of raw ultrasound data representations in deep learning to classify hepatic steatosis. *Ultrasound Med Biol*. 2022.
24. Baek J, Basavarajappa L, Hoyt K, Parker KJ. Disease-specific imaging utilizing support vector machine classification of H-scan parameters: assessment of steatosis in a rat model. *IEEE Trans Ultrason Ferroelectr Freq Control*. 2021;69(2):720-731.
25. Baek J, Qin SS, Prieto PA, Parker KJ, H-scan imaging and quantitative measurement to distinguish melanoma metastasis. Paper presented at: 2021 IEEE International Ultrasonics Symposium (IUS). 2021.
26. Baek J, Parker KJ, Disease-specific imaging with H-scan trajectories and support vector machine to visualize the progression of liver diseases. Paper presented at: 2021 IEEE International Ultrasonics Symposium (IUS). 2021.
27. Baek J, Parker KJ. H-scan trajectories indicate the progression of specific diseases. *Med Phys*. 2021;48(9):5047-5058.
28. Basavarajappa L, Li J, Tai H, Song J, Parker KJ, Hoyt K, Early detection of liver steatosis using multiparametric ultrasound imaging. Paper presented at: 2021 IEEE International Ultrasonics Symposium (IUS). 2021.
29. Schneider CA, Rasband WS, Eliceiri KW. NIH image to imageJ: 25 years of image analysis. *Nat Methods*. 2012;9(7):671-675.
30. Jayakumar S, Middleton MS, Lawitz EJ, et al. Longitudinal correlations between MRE, MRI-PDFF, and liver histology in patients with non-alcoholic steatohepatitis: analysis of data from a phase II trial of selonsertib. *J Hepatol*. 2019;70(1):133-141.
31. Baek J, Poul SS, Swanson TA, Tuthill T, Parker KJ. Scattering signatures of normal versus abnormal livers with support vector machine classification. *Ultrasound Med Biol*. 2020;46(12):3379-3392.
32. Basavarajappa L, Baek J, Reddy S, et al. Multiparametric ultrasound imaging for the assessment of normal versus steatotic livers. *Sci Rep-Uk*. 2021;11(1):1-11.

33. Murphy KP. *Machine learning: a probabilistic perspective*. MIT Press; 2012.
34. Molinaro AM, Simon R, Pfeiffer RM. Prediction error estimation: a comparison of resampling methods. *Bioinformatics*. 2005;21(15):3301-3307.
35. Garra BS, Shawker TH, Insana MF, Wagner RF, In vivo attenuation measurement: methods and clinical relevance. Paper presented at: Proceedings of the sixth EC workshop, Paris Ultrasonic Tissue characterisation. 6, 871986.
36. Parker KJ. Attenuation measurement uncertainties caused by speckle statistics. *J Acoust Soc Am*. 1986;80(3):727-734.
37. Tada T, Iijima H, Kobayashi N, et al. Usefulness of attenuation imaging with an ultrasound scanner for the evaluation of hepatic steatosis. *Ultrasound Med Biol*. 2019;45(10):2679-2687.
38. Gong P, Zhou CY, Song PF, et al. Ultrasound attenuation estimation in harmonic imaging for robust fatty liver detection. *Ultrasound Med Biol*. 2020;46(11):3080-3087.
39. Wen H, Zheng W, Li M, et al. Multiparametric quantitative US examination of liver fibrosis: a feature-engineering and machine-learning based analysis. *IEEE J Biomed Health Inform*. 2021;26(2):715-726.
40. Quiaoit K, DiCenzo D, Fatima K, et al. Quantitative ultrasound radiomics for therapy response monitoring in patients with locally advanced breast cancer: multi-institutional study results. *PLoS One*. 2020;15(7).
41. Reeder SB, Sirlin CB. Quantification of liver fat with magnetic resonance imaging. *Magnetic Reson Imaging Clin*. 2010;18(3):337-357.
42. Wildman-Tobriner B, Middleton MM, Moylan CA, et al. Association between magnetic resonance imaging–proton density fat fraction and liver histology features in patients with nonalcoholic fatty liver disease or nonalcoholic steatohepatitis. *Gastroenterology*. 2018;155(5):1428-1435. e1422.
43. Hu W, Yang H, Xu H, Mao Y. Radiomics based on artificial intelligence in liver diseases: where are we? *Gastroenterol Rep*. 2020;8(2):90-97.
44. Pavlides M, Banerjee R, Tunnicliffe EM, et al. Multiparametric magnetic resonance imaging for the assessment of non-alcoholic fatty liver disease severity. *Liver Int*. 2017;37(7):1065-1073.

How to cite this article: Baek J, Basavarajappa L, Margolis R, et al. Multiparametric ultrasound imaging for early-stage steatosis: Comparison with magnetic resonance imaging-based proton density fat fraction. *Med. Phys*. 2024;51:1313–1325.
https://doi.org/10.1002/mp.16648